NANO LETTERS

pubs.acs.org/NanoLett

Letter

# Observation of Terahertz-Induced Magnetooscillations in Graphene

Erwin Mönch,[▽] Denis A. Bandurin,[*,▽] Ivan A. Dmitriev,[▽] Isabelle Y. Phinney, Ivan Yahniuk, Takashi Taniguchi, Kenji Watanabe, Pablo Jarillo-Herrero, and Sergey D. Ganichev[*]

Cite This: *Nano Lett.* 2020, 20, 5943−5950

Read Online

ACCESS | Metrics & More | Article Recommendations | Supporting Information

**ABSTRACT:** When high-frequency radiation is incident upon graphene subjected to a perpendicular magnetic field, graphene absorbs incident photons by allowing transitions between nearest Landau levels that follow strict selection rules dictated by angular momentum conservation. Here, we show a qualitative deviation from this behavior in high-quality graphene devices exposed to terahertz (THz) radiation. We demonstrate the emergence of a pronounced THz-driven photoresponse, which exhibits low-field magnetooscillations governed by the ratio of the frequency of the incoming radiation and the quasiclassical cyclotron frequency. We analyze the modifications of generated photovoltage with the radiation frequency and carrier density and demonstrate that the observed photoresponse shares a common origin with microwave-induced resistance oscillations discovered in GaAs-based heterostructures; however, in graphene it appears at much higher frequencies and persists above liquid nitrogen temperatures. Our observations expand the family of radiation-driven phenomena in graphene, paving the way for future studies of nonequilibrium electron transport.

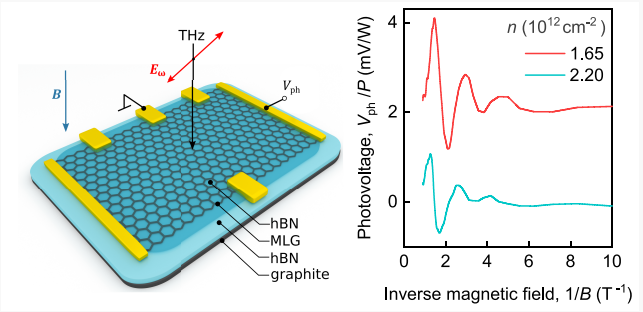


**KEYWORDS:** *graphene, terahertz radiation, microwave-induced resistance oscillations, photodetection, nonequilibrium transport, cyclotron resonance.*



In recent years, graphene has provided access to a rich variety of quantum effects, owing to its nontrivial band topology, quasi-relativistic energy spectrum, and high electron mobility.[1] These properties also determine the unique response of graphene to external electromagnetic fields: a host of interesting magneto-optical phenomena such as giant Faraday rotation,[2] radiation-driven nonlinear transport,[3] gate-tunable magnetoplasmons,[4,5] ratchet[6] and magnetic quantum ratchet effects,[7] as well as colossal magneto-absorption,[8,9] to name a few, has been discovered in graphene exposed to infrared and terahertz (THz) radiation. At these radiation frequencies, graphene also supports the propagation of long-lived gate-tunable plasmon-polaritons[10−13] enabling ultrahigh confinement of electromagnetic energy and offering a platform for the fundamental studies of radiation−matter interactions at the nanoscale.[14,15] Furthermore, in addition to fundamental interest, graphene's conical band structure together with fast carrier thermalization has generated much excitement for practical photonic and optoelectronic applications,[16] particularly for ultralong wavelengths.[17−20]

In this paper, we uncover a different kind of radiation-driven phenomena in graphene by studying the interplay of THz absorption with electron transport. We demonstrate that graphene subjected to a perpendicular magnetic field, $B$, exhibits pronounced $1/B$ magnetooscillations in response to incident THz-radiation. These magnetooscillations emerge in the range of weak magnetic fields well below those needed for the full development of conventional Shubnikov−de Haas oscillations, and their fundamental frequency is found to be proportional to the frequency of incoming radiation, $f$. By analyzing the observed THz-driven photovoltage as a function of gate-induced carrier density, $n$, we show that the resonant condition appears when $2\pi f$ is commensurate with the frequency of the electron's quasiclassical cyclotron motion, $\omega_c$. The latter indicates that the observed photovoltage oscillations have the same physical origin as the microwave-induced resistance oscillations (MIRO) in high-mobility 2DES with parabolic spectrum.[21−30] However, in graphene they emerge at higher frequencies and, quite remarkably, persist above liquid nitrogen temperatures, $T$, while their frequency is tunable by the gate voltage. Our observations expand the family of radiation-driven phenomena in graphene, paving the way for future studies of nonequilibrium electron transport.

**Received:** May 3, 2020
**Revised:** July 22, 2020
**Published:** July 22, 2020

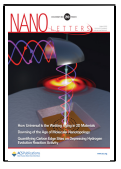

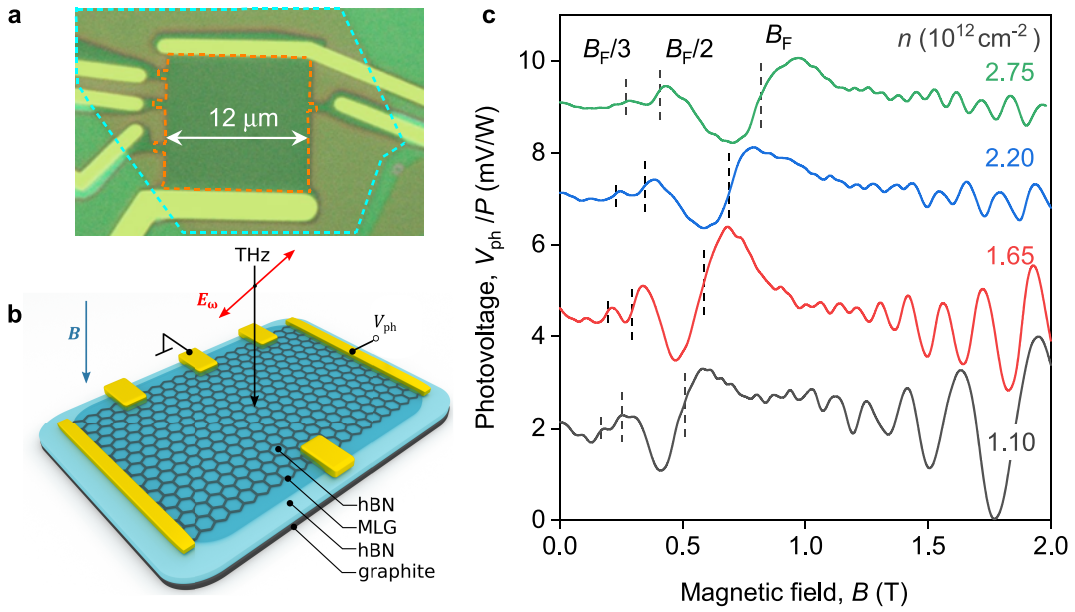


**Figure 1.** (a) Optical photograph of one of our encapsulated devices. Dashed red line highlights the shape of graphene Hall bar. Dashed blue line contours the graphite bottom gate region. (b) Measurement configuration: a normally incident THz laser radiation is focused on the graphene device placed in an out-of-plane magnetic field, $B$. Red and blue arrows show the in-plane polarization of the incident radiation and out-of-plane magnetic field. (c) Examples of the photovoltage dependence on the magnetic field recorded in response to 0.69 THz laser radiation at $T$ = 4.2 K. Different traces, corresponding to given carrier densities, $n$, are up-shifted for clarity. Dashed vertical lines at $B_F/N$, $N$ = 1, 2, 3, indicate harmonics of the cyclotron resonance in graphene, see eq 2.

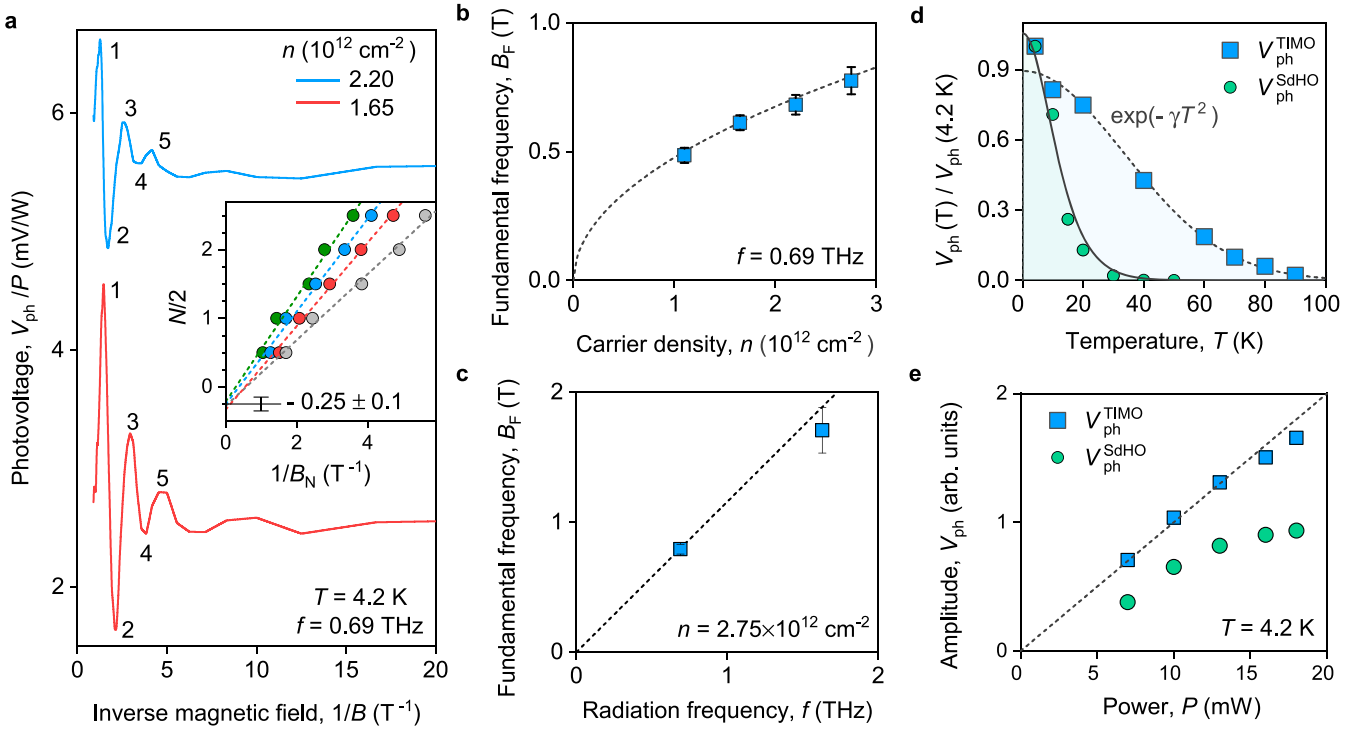


**Figure 2.** (a) Examples of TIMO in $V_{ph}$ as a function of inverse magnetic field for given $n$. Inset: TIMO extrema indices $N$ = 1,2,...5 (as marked) against the inverted values $1/B_N$ of magnetic field at which they appear. Color-coding is the same as in Figure 1c. Dashed lines: linear fits of the data used to determine the fundamental frequency $B_F$ (the slope) and the phase of TIMO, see eq 1. (b) $B_F$ as a function of $n$ for given $f$. (c) $B_F$ versus $f$ for given $n$. Dashed lines in (b,c): plots of $B_F(n,f)$ according to eq 2 with $v_F$ = 1.06 × $10^6$ m/s. (d) Temperature dependencies of the amplitude of the first period of TIMO ($V_{ph}^{TIMO}$, blue symbols) and of the SdHO-periodic photovoltage ($V_{ph}^{SdHO}$, green symbols) for $n$ = 2.75 × $10^{12}$ cm$^{-2}$. Solid black line: Fit of $V_{ph}^{SdHO}$ to the Lifshitz-Kosevich formula yielding $m_c \approx 0.03m_e$ where $m_e$ is the free electron mass. Dashed black line: fit of $V_{ph}^{TIMO}$ for $T \geq 10$ K with the function $\exp(-\gamma T^2)$ yielding $\gamma$ = 4.4 × $10^{-4}$ K$^{-2}$. (e) Incident THz power dependencies of $V_{ph}^{TIMO}$ (blue symbols) and $V_{ph}^{SdHO}$ (green symbols). Dashed black line: linear fit to the data.



https://dx.doi.org/10.1021/acs.nanolett.0c01918
Nano Lett. 2020, 20, 5943−5950

## DEVICES AND MEASUREMENTS

Our samples are multiterminal devices made of monolayer graphene (MLG) encapsulated between two crystals of hexagonal boron nitride (hBN) fabricated using a high-temperature release method.[31] The devices were patterned in a conventional Hall bar geometry and transferred on top of a graphite flake, Figure 1a,b, see Supporting Information for details. The latter served as a gate electrode controlling the concentration, $n$, and was also used to screen the remote charged impurities in $Si/SiO_2$ substrate.[32] The devices had a width of 12 $\mu$m and exhibited high mobility, $\mu$, exceeding $3 \times 10^5$ cm$^2$/(V s) at $T = 4.2$ K.

Experiments were performed in a variable temperature optical cryostat with polyethylene windows to allow coupling of the sample with linearly polarized THz radiation. The latter was generated by a continuous wave molecular gas laser operating at frequencies $f = 0.69$ and 1.63 THz with radiation power up to 20 mW.[33,34] By using a pyroelectric camera,[35] the laser spot with diameter of about 2.5 mm was guided to the center of the device. Note that the size of the laser spot largely exceeding the sample size leaves a possibility of antenna effects produced by the contact wires. The THz beam was modulated by an optical chopper operating at a frequency of about 80 Hz. Photovoltage, $V_{ph}$, was recorded as a phase-locked potential difference between a pair of contacts of the unbiased sample generated in response to the chopper-modulated THz radiation, using a standard lock-in technique. For all gate voltages, the sample resistance was much smaller than 10 MΩ input resistance of the lock-in amplifier (Supporting Information). All data were obtained in Faraday configuration (Figure 1b) with both the laser beam and magnetic field oriented perpendicular to the graphene plane.

The central result of our study is presented in Figure 1c, which shows the emergence of $V_{ph}$ in response to $f = 0.69$ THz radiation when a magnetic field, $B$, perpendicular to graphene is applied. Different traces correspond to several representative values of $n$. Two kinds of magnetooscillations are clearly distinct in the data. At $B > 1$ T, $V_{ph}$ exhibits fast $1/B$-periodic oscillations which display periodicity of conventional Shubnikov–de Haas oscillations (SdHO). The presence of SdHO-periodic signals in the photovoltage is not surprising and is in line with previous observations.[36,37] Strikingly, at lower $B < 1$ T, where the SdHO-periodic oscillations become exponentially suppressed, another distinct magneto-oscillation pattern emerges. These low-$B$ oscillations, for brevity denoted THz-induced magnetooscillations (TIMO), will be explored in the remainder of this paper.

In Figure 2a, we replot two examples of $V_{ph}$ from Figure 2a as a function of inverse magnetic field. Both traces clearly indicate the $1/B$-periodicity of TIMO. This periodicity is further verified by plotting the indices $N = 1, 2,...5$ of the consecutive peaks and dips, see Figure 2a, against the values $1/B_N$ of the inverse magnetic field at which they appear. As demonstrated in the inset of Figure 2a, for each $n$ in Figure 1c the positions of all extrema fall onto straight lines. The slope of these lines yields the fundamental frequency of TIMO, $B_F$, which varies with $n$ and $f$, as shown in Figure 2b,c (for further details, see Supporting Information). Moreover, all lines cross the vertical axis at the same point, $-0.25 \pm 0.1$. This behavior yields the relation $N/2 = B_F/B_N - 1/4$, which translates into

$$V_{ph}^{TIMO} \propto -\sin\left(\frac{2\pi B_F}{B}\right) \quad (1)$$

and thus establishes the TIMO phase, which will be important for the further analysis.

We have also studied $V_{ph}(B)$ at different temperatures and found that the amplitudes of SdHO-periodic oscillations and TIMO exhibit very different $T$-dependences as shown in Figure 2d (for further details, see Supporting Information). Remarkably, we observe that TIMO, and in particular their first period, can be well resolved even above liquid nitrogen temperatures in sharp contrast to the SdHO-periodic signal, which vanishes completely at $T \sim 40$ K over the entire $B$- and $n$- ranges in which the measurements were performed. The latter dependence can be well fitted by the conventional Lifshitz-Kosevich formula[38,39] as illustrated by the solid line.

The evolution of TIMO and SdHO-periodic signals with the power of incident THz radiation, $P$, is also found to be different, see Figure 2e. The $P$-dependence of the TIMO amplitude is fairly linear with a weak tendency to saturation at the highest $P > 10$ mW. This means that much stronger TIMO can be observed using more powerful THz sources. In contrast to TIMO, the amplitude of SdHO-periodic photoresponse clearly displays a sublinear $P$-dependence, which may reflect the electron heating caused by the THz irradiation.

## MIRO PHYSICS IN GRAPHENE DEVICES

Below we argue that the above experimental results identify TIMO as a graphene analogue of microwave-induced resistance oscillations (MIRO).[21−25,29,30,40−45] The maxima and minima of MIRO appear around the positions of harmonics of the cyclotron resonance (CR) given by $\omega = M\omega_c$, where $\omega = 2\pi f$, $M = 1, 2...$, and $\omega_c = eB/m$ is the cyclotron frequency.[46] It is thus natural to attribute this effect to resonant photon-assisted transitions between distant Landau levels (LLs).[47−51] Such processes require simultaneous impurity scattering,[49−51] since in the absence of disorder only transitions between neighboring LLs ($M = 1$) are dipole-allowed. Indeed, MIRO are observed in the range of $B$ where LLs are strongly broadened by disorder, see Figure 3a. This is reflected in an exponential decay toward low $B$ that is similar to the SdHO and other quantum corrections to the classical Drude-Boltzmann transport coefficients.[30,39]

In order to understand how the above photon-assisted transitions between broadened LLs lead to magnetooscillations in static transport observables such as photoconductivity[52] and photovoltage,[53] a theoretical framework involving two closely related mechanisms, referred to as displacement[54−58] and inelastic,[50,59] has been developed (for other theoretical proposals, see refs 60−63). A hallmark of both mechanisms is that the effect vanishes at exact positions of the CR harmonics. We demonstrate this in Figure 3a, which illustrates the displacement mechanism. Solid lines show the maxima of the local density of states (DOS) in broadened LLs (shown on the left) which are tilted in the presence of a static electric field $\mathbf{E}$. Note that $\mathbf{E}$ here represents the local gradient of electrostatic potential, which can still be present in the absence of external dc driving due to an asymmetry of contact configuration or intrinsic inhomogeneities, thus leading to oscillatory photocurrent and/or photovoltage.[26−28,53,64] In a magnetic field, any impurity scattering is accompanied by a real-space displacement $\Delta\mathbf{X}$ of the center of the electron cyclotron orbit. In the example of Figure 3a, the photon energy


https://dx.doi.org/10.1021/acs.nanolett.0c01918
Nano Lett. 2020, 20, 5943−5950

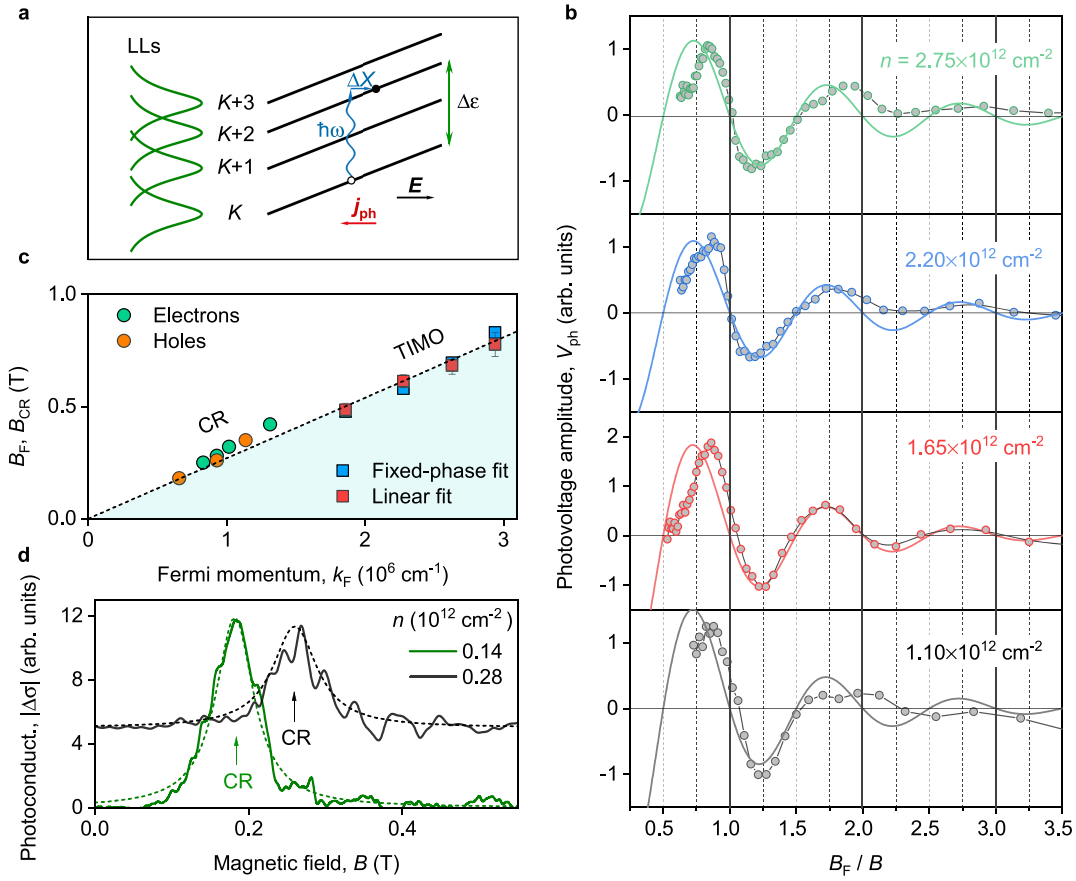


**Figure 3.** (a) Schematic for the displacement mechanism of MIRO. Solid lines show how the energy positions of the centers of broadened LLs (shown on the left) are shifted in real space in the presence of a static electric field **E**. The impurity-assisted photon absorption leads to an inter-LL transition accompanied by a real space displacement of electron's cyclotron orbit, $\Delta\mathbf{X}$. The preferred direction of $\Delta\mathbf{X}$ is sensitive to the final density of states available for scattering. On the schematic, the photon energy $\hbar\omega$ slightly exceeds the distance $\Delta\varepsilon$ between the involved LLs, and the density of the final states is larger for the spatial shifts in the direction of **E**. This results in the generation of the photocurrent $\mathbf{j}_{ph}$ in the opposite direction. (b) Circles: Low-field $V_{ph}$ as a function of $B_F/B$ after subtraction of nonoscillating background (obtained by using running average with the windows size larger than the oscillations period). Solid lines: fits to eq 3. The value of $B_F$ for each carrier density is chosen to provide the best fit for the period of TIMO with the phase fixed by eq 3. (c) $B_F$ as a function of $k_F$ determined by the fixed-phase fits to eq 3 (blue squares) and the linear fits in Figure 2a (red squares). Dashed line shows the fit of $B_F$ values obtained via both methods to $B_F = \hbar\omega k_F/ev_F$, yielding $v_F = (1.06 \pm 0.06) \times 10^6$ m/s. Circles mark the positions $B_{CR}$ of the CR peaks detected in the photoconductivity at small $|n|$, see panel (d). (d) Examples of photoconductivity $|\Delta\sigma|$ versus $B$ dependencies demonstrating pronounced quasi-classical CR at given $n$. Solid lines: Lorentzian fits to the data used to determine $B_{CR}$ (arrows) shown in panel (c). The curves are shifted for clarity. $T = 4.2$ K.

$\hbar\omega$ slightly exceeds the energy separation $\Delta\varepsilon$ between the involved LLs. This defines the preferred direction of the displacement $\Delta\mathbf{X}$ due to the photon-assisted impurity scattering and, consequently, the oppositely directed contribution to the photocurrent $\mathbf{j}_{ph}$. As one would expect from golden rule arguments,[30,54] the statistically averaged displacement vector points to the right, toward the maximum in the local DOS associated with the $K + 2$LL. The direction of $\Delta\mathbf{X}$ would reverse for the opposite sign of $\hbar\omega - \Delta\varepsilon$ and, therefore, the nonequilibrium current $\mathbf{j}_{ph}$ can flow both along and against **E**, depending on the sign of $\hbar\omega - \Delta\varepsilon$, and vanishes at the positions of CR harmonics.

In addition to $\mathbf{j}_{ph}$ associated with such displacements of orbits, the resonant inter-LL transitions lead to an unusual modification of the Fermi–Dirac energy distribution of electrons, which acquires a nonequilibrium correction proportional to the oscillatory DOS.[50,65] Since the amplitude of oscillations in the energy distribution is controlled by inelastic scattering processes, the corresponding contribution to MIRO[59] is termed inelastic. Both displacement and inelastic mechanisms lead to a violation of the Einstein relation between diffusion coefficient and conductivity thus producing similar contributions to the photoconductivity and photocurrent.[53,64]

In 2DES with a parabolic energy dispersion, the LL spectrum is equidistant, and MIRO display $2\pi$-periodicity with the ratio $\omega/\omega_c \equiv m\omega/eB$. The fundamental frequency of MIRO, $B_F = m\omega/e$, is thus insensitive to variations of the electron density, neglecting small changes of the effective mass $m$ due to density-dependent renormalization induced by electron–electron interactions.[66,67] This property should clearly change in graphene, which features a nonequidistant spectrum of LLs, $E_K \propto \sqrt{K}$, $K = 0, 1, 2...$[68] In a narrow energy window of $\max\{\hbar\omega, k_BT\} \ll E_F$ around the chemical potential $E_F$, which is available for impurity-assisted emission and absorption of photons, the spacing between LLs at relevant $K \gg 1$ can be still approximated as $\hbar\omega_c = \hbar eB/m_c$ but with the density-dependent cyclotron mass $m_c = \hbar\sqrt{\pi n}/v_F$.[69] Therefore, the fundamental frequency of TIMO


https://dx.doi.org/10.1021/acs.nanolett.0c01918
Nano Lett. 2020, 20, 5943–5950

$$B_F = \frac{\hbar\omega\sqrt{\pi n}}{e v_F} \quad (2)$$

is expected to scale with $\sqrt{n}$. These expectations are in excellent agreement with our findings; dashed lines in Figure 2b,c demonstrate that the fundamental frequency of TIMO accurately follows eq 2 as a function of $n$ and $\omega$ if one uses $v_F = 1.06 \times 10^6$ m/s typical for the relevant range of densities in graphene.[69−71]

TIMO also displays other common features with MIRO, including the vanishing photoresponse at integer $B_F/B$ (see vertical dashed lines in Figure 1c) and an exponential damping toward low $B$. These further manifestations of the MIRO phenomenon are evident from Figure 3b, which compares the TIMO data with the conventional MIRO waveform

$$V_{ph} = -A \exp\left(-\frac{\alpha B_F}{B}\right)\sin\left(\frac{2\pi B_F}{B}\right) \quad (3)$$

typical for weak oscillations in the regime of strongly overlapping LLs and small radiation intensity.[30,72] The solid lines in Figure 3b are fits to eq 3 with constants $A$, $B_{CR}$, and $\alpha$ used as fitting parameters. This treatment complements the procedure presented in Figure 2a, where the phase of TIMO was not fixed as in eq 3 but rather emerged as a result of the analysis, see eq 1. The values of $B_F$, obtained using either of the two fitting procedures, nearly coincide. They are plotted together as a function of the Fermi momentum $k_F = \sqrt{\pi n}$ in Figure 3c and exhibit the proportionality to $k_F$ in accordance with eq 2. A fit for the slope yields the value $v_F = (1.06 \pm 0.06) \times 10^6$ m/s which is in good agreement with previous studies.[1]

Our observations establish that despite their resonant character, TIMO vanish at the exact position $B = B_F$ of the cyclotron resonance (CR). This makes them markedly different from more conventional effects in the photoresponse, which are related to the resonant heating of electrons due to enhanced Drude absorption near the CR.[67] Such CR-enhanced photoresponse was also detected in our devices but at small $|n|$ where TIMO were not observed. Two examples of the photoconductivity, $\Delta\sigma$, traces featuring the CR-centered peaks are shown in Figure 3d. The positions $B_{CR}$ of these CR peaks are included in Figure 3c. They fall onto the dashed line representing $B_F(k_F)$ dependence extracted from TIMO and further substantiate the previous analysis.

## DAMPING OF THZ-INDUCED MAGNETOOSCILLATIONS IN GRAPHENE

We now focus our attention on the low-$B$ damping and $T$-dependence of TIMO, which turn out to be closely interrelated. Fitting the low-$T$ TIMO data using eq 3, see Figure 3b, we find that the low-$B$ damping of TIMO is well reproduced by the factor $\exp(-\alpha B_F/B)$ with $\alpha \simeq 1$. This factor describes an increasing overlap of the broadened LLs upon lowering $B$,[52] and can be rewritten as the square, $\delta^2$, of the conventional Dingle factor $\delta = \exp(-\pi/\omega_c\tau_q)$. Remarkably, the corresponding value of the quantum scattering time, $\tau_q = 1/\alpha f \simeq 1.5$ ps, significantly exceeds the values $\tau_q \sim 0.3$ ps extracted from the SdHO measurements in graphene samples of similar quality[73] yet is a few times smaller than typical low-$T$ values $\tau_{tr} \sim 5-10$ ps of the transport scattering time in our samples. The obtained scattering times are at least an order of magnitude shorter than those of the GaAs-based heterostructures used to study MIRO.[30] In view of the relation $\alpha = 1/f\tau_q$, this necessitates the use of higher (THz) frequencies in graphene to observe nonequilibrium phenomena of this type. On the other hand, calculations show that an increase of the radiation frequency causes a very fast $f^{-4}$ decay in MIRO amplitude $A$, as opposed to a slower $f^{-2}$ decay of the Drude absorption and associated electron heating.[30] The observation of the MIRO-like oscillations in conventional 2DES thus proved challenging for $f$ above 1 THz.[74,75] Our samples, in contrast, revealed clear signatures of TIMO at elevated THz frequencies (see Figure 2c and Supporting Information), which points to an exceptional stability of TIMO against heating effects.

The anomalously slow $T$-decay of TIMO is also not less intriguing. At elevated $T$, electron−electron (e-e) collisions can provide an additional contribution $1/f\tau_{ee} \equiv \gamma T^2$ to the damping parameter $\alpha$ in eq 3.[52,76−78] The relevant lifetime $\tau_{ee}$, responsible for the effective broadening of LLs, is given by the Fermi-liquid e-e scattering rate,[79,80] $\tau_{ee}^{-1} = cT^2/\varepsilon_F\hbar$, where $\varepsilon_F$ denotes the Fermi energy, and constant $c$ of order unity includes the logarithmic and numerical factors.[52,59] Our data presented in Figure 2d reveal that this effect dominates the $T$-dependence of TIMO in the majority of the studied interval of $T$. Indeed, at $T \sim 10$ K the amplitude of TIMO around $B = B_F$ precisely follows the exponential fit $\exp(-\gamma T^2)$. Moreover, the value of $\tau_{ee} \simeq (57\ \mathrm{K}/T)^2$ ps extracted from this fit conforms with both experimental values reported for graphene[81] (Supporting Information) and the above theoretical estimate (with a reasonable value of $c \simeq 5.6$).[82,83] The above analysis suggests that the parameter $A$ in eq 3 remains approximately independent of $T$ in the range $T > 10$ K. Such behavior, consistent with the $\exp(-\gamma T^2)$ decay, is characteristic for the displacement mechanism described above[76,77] (Supporting Information). We also note that recently observed magneto-phonon oscillations (resonant phonon-assisted inter-LL transitions) in graphene[71,84] also exhibited similarly slow $T$-decay; these can potentially be accounted for by e-e scattering as well.[85]

It is instructive to point out that the relevant Fermi energy $\varepsilon_F \sim 200$ meV in graphene is ∼20 times larger than the standard values in GaAs-based heterostructures used for measurements of MIRO. Together with the ∼10 times larger frequency $f = 0.69$ THz, this explains why the decay parameter $\gamma \propto 1/f\varepsilon_F$ is more than 100 times smaller in graphene.

To conclude, we have demonstrated the emergence of strong magnetooscillations in graphene exposed to THz radiation. The oscillations were found to have a common origin with MIRO phenomena observed in 2DES with parabolic spectrum, but they emerge at much higher $f$, persist above liquid nitrogen temperatures, and their fundamental frequency is tunable by the gate voltage. The anomalously slow $T$-decay of the observed oscillations compared to other 2DES was demonstrated to be due to a slower rate of e-e scattering responsible for the broadening of LLs. As an outlook, we note that the linear growth of the oscillation amplitude with increasing power can offer an intriguing opportunity to explore further radiation-driven effects. In particular, the observation of zero resistance states[23,24,86] in THz-driven graphene together with nonlinear response of Dirac fermions[87] may pave the way for a deeper understanding of the rich spectra of non-equilibrium phenomena in 2DES and help to resolve the remaining open questions.[30,40,43,74,88]



https://dx.doi.org/10.1021/acs.nanolett.0c01918
Nano Lett. 2020, 20, 5943−5950

## ■ ASSOCIATED CONTENT

### Supporting Information

The Supporting Information is available free of charge at https://pubs.acs.org/doi/10.1021/acs.nanolett.0c01918.

Details on device fabrication, TIMO for different THz frequencies, temperatures, and contact pairs, photogalvanics at $B = 0$, and magnetotransport (PDF)

## ■ AUTHOR INFORMATION


### Corresponding Authors

**Denis A. Bandurin** − *Department of Physics, Massachusetts Institute of Technology, Cambridge, Massachusetts 02139, United States*; Email: bandurin@mit.edu

**Sergey D. Ganichev** − *Terahertz Center, University of Regensburg, 93040 Regensburg, Germany*; orcid.org/0000-0001-6423-4509; Email: sergey.ganichev@ur.de

### Authors

**Erwin Mönch** − *Terahertz Center, University of Regensburg, 93040 Regensburg, Germany*

**Ivan A. Dmitriev** − *Terahertz Center, University of Regensburg, 93040 Regensburg, Germany; Ioffe Institute, 194021 St. Petersburg, Russia*

**Isabelle Y. Phinney** − *Department of Physics, Massachusetts Institute of Technology, Cambridge, Massachusetts 02139, United States*

**Ivan Yahniuk** − *CENTERA, Institute of High Pressure Physics PAS, 01142 Warsaw, Poland*

**Takashi Taniguchi** − *International Center for Materials Nanoarchitectonics, National Institute of Material Science, Tsukuba 305-0044, Japan*; orcid.org/0000-0002-1467-3105

**Kenji Watanabe** − *Research Center for Functional Materials, National Institute of Material Science, Tsukuba 305-0044, Japan*; orcid.org/0000-0003-3701-8119

**Pablo Jarillo-Herrero** − *Department of Physics, Massachusetts Institute of Technology, Cambridge, Massachusetts 02139, United States*

Complete contact information is available at: https://pubs.acs.org/10.1021/acs.nanolett.0c01918

### Author Contributions

[▽]E.M., D.A.B., and I.A.D. contributed equally to this work.


### Notes

The authors declare no competing financial interest.

## ■ ACKNOWLEDGMENTS

The support from the Deutsche Forschungsgemeinschaft (DFG, German Research Foundation), Project GA501/14-1, the Volkswagen Stiftung Program (97738), and the IRAP program of the Foundation for Polish Science (Grant MAB/2018/9, project CENTERA) is gratefully acknowledged. The research was also partially supported through the TEAM project POIR.04.04.00-00-3D76/16 (TEAM/2016-3/25) of the Foundation for Polish Science. Work at MIT was partly supported through AFOSR Grant FA9550-16-1-0382, through the NSF QII-TAQS program (Grant 1936263), and the Gordon and Betty Moore Foundation EPiQS Initiative through Grant GBMF4541 to P.J.H. This work made use of the Materials Research Science and Engineering Center Shared Experimental Facilities supported by the National Science Foundation (NSF) (Grant DMR-0819762). D. A. B. acknowledges support from MIT Pappalardo fellowship. Growth of hBN crystals was supported by the Elemental Strategy Initiative conducted by the MEXT, Japan, Grant JPMXP0112101001, JSPS KAKENHI Grant JP20H00354, and the CREST (JPMJCR15F3), JST. The authors thank valuable discussions with D. Svintsov and L. Levitov.

## ■ REFERENCES


(1) Castro Neto, A. H.; Guinea, F.; Peres, N. M. R.; Novoselov, K. S.; Geim, A. K. The electronic properties of graphene. *Rev. Mod. Phys.* **2009**, *81*, 109−162.

(2) Crassee, I.; Levallois, J.; Walter, A. L.; Ostler, M.; Bostwick, A.; Rotenberg, E.; Seyller, T.; van der Marel, D.; Kuzmenko, A. B. Giant Faraday rotation in single- and multilayer graphene. *Nat. Phys.* **2011**, *7*, 48−51.

(3) Glazov, M. M.; Ganichev, S. D. High frequency electric field induced nonlinear effects in graphene. *Phys. Rep.* **2014**, *535*, 101.

(4) Crassee, I.; Orlita, M.; Potemski, M.; Walter, A. L.; Ostler, M.; Seyller, T.; Gaponenko, I.; Chen, J.; Kuzmenko, A. B. Intrinsic terahertz plasmons and magnetoplasmons in large scale monolayer graphene. *Nano Lett.* **2012**, *12*, 2470.

(5) Yan, H.; Li, Z.; Li, X.; Zhu, W.; Avouris, P.; Xia, F. Infrared spectroscopy of tunable dirac terahertz magneto-plasmons in graphene. *Nano Lett.* **2012**, *12*, 3766.

(6) Olbrich, P.; et al. Terahertz ratchet effects in graphene with a lateral superlattice. *Phys. Rev. B: Condens. Matter Mater. Phys.* **2016**, *93*, No. 075422.

(7) Drexler, C.; et al. Magnetic quantum ratchet effect in graphene. *Nat. Nanotechnol.* **2013**, *8*, 104−107.

(8) Jiang, Z.; Henriksen, E. A.; Tung, L. C.; Wang, Y.-J.; Schwartz, M. E.; Han, M. Y.; Kim, P.; Stormer, H. L. Infrared spectroscopy of Landau levels of graphene. *Phys. Rev. Lett.* **2007**, *98*, 197403.

(9) Nedoliuk, I. O.; Hu, S.; Geim, A. K.; Kuzmenko, A. B. Colossal infrared and terahertz magneto-optical activity in a two-dimensional Dirac material. *Nat. Nanotechnol.* **2019**, *14*, 756−761.

(10) Ju, L.; Geng, B.; Horng, J.; Girit, C.; Martin, M.; Hao, Z.; Bechtel, H. A.; Liang, X.; Zettl, A.; Shen, Y. R.; Wang, F. Graphene plasmonics for tunable terahertz metamaterials. *Nat. Nanotechnol.* **2011**, *6*, 630−634.

(11) Alonso-González, P.; et al. Acoustic terahertz graphene plasmons revealed by photocurrent nanoscopy. *Nat. Nanotechnol.* **2017**, *12*, 31−35.

(12) Grigorenko, A. N.; Polini, M.; Novoselov, K. S. Graphene plasmonics. *Nat. Photonics* **2012**, *6*, 749−758.

(13) Bandurin, D. A.; Svintsov, D.; Gayduchenko, I.; Xu, S. G.; Principi, A.; Moskotin, M.; Tretyakov, I.; Yagodkin, D.; Zhukov, S.; Taniguchi, T.; Watanabe, K.; Grigorieva, I. V.; Polini, M.; Goltsman, G. N.; Geim, A. K.; Fedorov, G. Resonant terahertz detection using graphene plasmons. *Nat. Commun.* **2018**, *9*, 5392.

(14) Lundeberg, M. B.; Gao, Y.; Asgari, R.; Tan, C.; Van Duppen, B.; Autore, M.; Alonso-González, P.; Woessner, A.; Watanabe, K.; Taniguchi, T.; Hillenbrand, R.; Hone, J.; Polini, M.; Koppens, F. H. L. Tuning quantum nonlocal effects in graphene plasmonics. *Science* **2017**, *357*, 187−191.

(15) Ni, G. X.; McLeod, A. S.; Sun, Z.; Wang, L.; Xiong, L.; Post, K. W.; Sunku, S. S.; Jiang, B. Y.; Hone, J.; Dean, C. R.; Fogler, M. M.; Basov, D. N. Fundamental limits to graphene plasmonics. *Nature* **2018**, *557*, 530−533.

(16) Bonaccorso, F.; Sun, Z.; Hasan, T.; Ferrari, A. C. Graphene photonics and optoelectronics. *Nat. Photonics* **2010**, *4*, 611−622.

(17) Rogalski, A.; Kopytko, M.; Martyniuk, P. Two-dimensional infrared and terahertz detectors: Outlook and status. *Appl. Phys. Rev.* **2019**, *6*, No. 021316.

(18) Koppens, F. H. L.; Mueller, T.; Avouris, P.; Ferrari, A. C.; Vitiello, M. S.; Polini, M. Photodetectors based on graphene, other two-dimensional materials and hybrid systems. *Nat. Nanotechnol.* **2014**, *9*, 780−793.

(19) Jung, M.; Rickhaus, P.; Zihlmann, S.; Makk, P.; Schönenberger, C. Microwave photodetection in an ultraclean suspended bilayer graphene p−n junction. *Nano Lett.* **2016**, *16*, 6988−6993.
(20) Lee, G.-H.; Efetov, D. K.; Ranzani, L.; Walsh, E. D.; Ohki, T. A.; Taniguchi, T.; Watanabe, K.; Kim, P.; Englund, D.; Fong, K. C. Graphene-based Josephson junction microwave bolometer. 2019, 1909.05413. arXiv/cond-mat.mes-hall. https://arxiv.org/abs/1909.05413v2/ (accessed October 18, 2019).
(21) Zudov, M. A.; Du, R. R.; Simmons, J. A.; Reno, J. L. Shubnikov−de Haas-like oscillations in millimeterwave photoconductivity in a high-mobility two-dimensional electron gas. *Phys. Rev. B: Condens. Matter Mater. Phys.* **2001**, *64*, 201311.
(22) Ye, P. D.; Engel, L. W.; Tsui, D. C.; Simmons, J. A.; Wendt, J. R.; Vawter, G. A.; Reno, J. L. Giant microwave photoresistance of two-dimensional electron gas. *Appl. Phys. Lett.* **2001**, *79*, 2193.
(23) Mani, R. G.; Smet, J. H.; von Klitzing, K.; Narayanamurti, V.; Johnson, W. B.; Umansky, V. Zero-resistance states induced by electromagnetic-wave excitation in GaAs/AlGaAs heterostructures. *Nature* **2002**, *420*, 646.
(24) Zudov, M. A.; Du, R. R.; Pfeiffer, L. N.; West, K. W. Evidence for a New Dissipationless Effect in 2D Electronic Transport. *Phys. Rev. Lett.* **2003**, *90*, No. 046807.
(25) Yang, C. L.; Zudov, M. A.; Knuuttila, T. A.; Du, R. R.; Pfeiffer, L. N.; West, K. W. Observation of microwave-induced zero-conductance state in Corbino rings of a two-dimensional electron system. *Phys. Rev. Lett.* **2003**, *91*, No. 096803.
(26) Willett, R. L.; Pfeiffer, L. N.; West, K. W. Evidence for current-flow anomalies in the irradiated 2D electron system at small magnetic fields. *Phys. Rev. Lett.* **2004**, *93*, No. 026804.
(27) Bykov, A. A. Microwave-induced magnetic field oscillations of the electromotive force in a two-dimensional Corbino disk at large filling factors. *JETP Lett.* **2008**, *87*, 233.
(28) Dorozhkin, S. I.; Pechenezhskiy, I. V.; Pfeiffer, L. N.; West, K. W.; Umansky, V.; von Klitzing, K.; Smet, J. H. Photocurrent and Photovoltage Oscillations in the Two-Dimensional Electron System: Enhancement and Suppression of Built-In Electric Fields. *Phys. Rev. Lett.* **2009**, *102*, No. 036602.
(29) Kärcher, D. F.; Shchepetilnikov, A. V.; Nefyodov, Y. A.; Falson, J.; Dmitriev, I. A.; Kozuka, Y.; Maryenko, D.; Tsukazaki, A.; Dorozhkin, S. I.; Kukushkin, I. V.; Kawasaki, M.; Smet, J. H. Observation of microwave induced resistance and photovoltage oscillations in MgZnO/ZnO heterostructures. *Phys. Rev. B: Condens. Matter Mater. Phys.* **2016**, *93*, No. 041410.
(30) Dmitriev, I. A.; Mirlin, A. D.; Polyakov, D. G.; Zudov, M. A. Nonequilibrium phenomena in high Landau levels. *Rev. Mod. Phys.* **2012**, *84*, 1709−1763.
(31) Purdie, D. G.; Pugno, N. M.; Taniguchi, T.; Watanabe, K.; Ferrari, A. C.; Lombardo, A. Cleaning interfaces in layered materials heterostructures. *Nat. Commun.* **2018**, *9*, 5387.
(32) Zibrov, A. A.; Kometter, C.; Zhou, H.; Spanton, E. M.; Taniguchi, T.; Watanabe, K.; Zaletel, M. P.; Young, A. F. Tunable interacting composite fermion phases in a half-filled bilayer-graphene Landau level. *Nature* **2017**, *549*, 360−364.
(33) Danilov, S. N.; Wittmann, B.; Olbrich, P.; Eder, W.; Prettl, W.; Golub, L. E.; Beregulin, E. V.; Kvon, Z. D.; Mikhailov, N. N.; Dvoretsky, S. A.; Shalygin, V. A.; Vinh, N. Q.; van der Meer, A. F. G.; Murdin, B.; Ganichev, S. D. Fast detector of the ellipticity of infrared and terahertz radiation based on HgTe quantum well structures. *J. Appl. Phys.* **2009**, *105*, No. 013106.
(34) Olbrich, P.; Zoth, C.; Vierling, P.; Dantscher, K.-M.; Budkin, G. V.; Tarasenko, S. A.; Bel'kov, V. V.; Kozlov, D. A.; Kvon, Z. D.; Mikhailov, N. N.; Dvoretsky, S. A.; Ganichev, S. D. Giant photocurrents in a Dirac fermion system at cyclotron resonance. *Phys. Rev. B: Condens. Matter Mater. Phys.* **2013**, *87*, 235439.
(35) Ziemann, E.; Ganichev, S. D.; Prettl, W.; Yassievich, I. N.; Perel, V. I. Characterization of deep impurities in semiconductors by terahertz tunneling ionization. *J. Appl. Phys.* **2000**, *87*, 3843−3849.
(36) Cao, H.; Aivazian, G.; Fei, Z.; Ross, J.; Cobden, D. H.; Xu, X. Photo-Nernst current in graphene. *Nat. Phys.* **2016**, *12*, 236−239.
(37) Zoth, C.; Olbrich, P.; Vierling, P.; Dantscher, K.-M.; Bel'kov, V. V.; Semina, M. A.; Glazov, M. M.; Golub, L. E.; Kozlov, D. A.; Kvon, Z. D.; Mikhailov, N. N.; Dvoretsky, S. A.; Ganichev, S. D. Quantum oscillations of photocurrents in HgTe quantum wells with Dirac and parabolic dispersions. *Phys. Rev. B: Condens. Matter Mater. Phys.* **2014**, *90*, 205415.
(38) Shoenberg, D. *Magnetic oscillations in metals*; Cambridge Monographs on Physics; Cambridge University Press: Cambridge, 1984; Vol. *1*, p 153.
(39) Ando, T.; Fowler, A. B.; Stern, F. Electronic properties of two-dimensional systems. *Rev. Mod. Phys.* **1982**, *54*, 437.
(40) Smet, J. H.; Gorshunov, B.; Jiang, C.; Pfeiffer, L.; West, K.; Umansky, V.; Dressel, M.; Meisels, R.; Kuchar, F.; von Klitzing, K. Circular-polarization-dependent study of the microwave photoconductivity in a two-dimensional electron system. *Phys. Rev. Lett.* **2005**, *95*, 116804.
(41) Zudov, M. A.; Mironov, O. A.; Ebner, Q. A.; Martin, P. D.; Shi, Q.; Leadley, D. R. Observation of microwave-induced resistance oscillations in a high-mobility two-dimensional hole gas in a strained Ge/SiGe quantum well. *Phys. Rev. B: Condens. Matter Mater. Phys.* **2014**, *89*, 125401.
(42) Yamashiro, R.; Abdurakhimov, L. V.; Badrutdinov, A. O.; Monarkha, Y. P.; Konstantinov, D. Photoconductivity response at cyclotron-resonance harmonics in a nondegenerate two-dimensional electron gas on liquid Helium. *Phys. Rev. Lett.* **2015**, *115*, 256802.
(43) Zadorozhko, A. A.; Monarkha, Y. P.; Konstantinov, D. Circular-polarization-dependent study of microwave-induced conductivity oscillations in a two-dimensional electron gas on liquid Helium. *Phys. Rev. Lett.* **2018**, *120*, No. 046802.
(44) Otteneder, M.; Dmitriev, I. A.; Candussio, S.; Savchenko, M. L.; Kozlov, D. A.; Bel'kov, V. V.; Kvon, Z. D.; Mikhailov, N. N.; Dvoretsky, S. A.; Ganichev, S. D. Sign-alternating photoconductivity and magnetoresistance oscillations induced by terahertz radiation in HgTe quantum wells. *Phys. Rev. B: Condens. Matter Mater. Phys.* **2018**, *98*, 245304.
(45) Monarkha, Y.; Konstantinov, D. Magneto-oscillations and anomalous current states in a photoexcited electron gas on liquid Helium. *J. Low Temp. Phys.* **2019**, *197*, 208.
(46) Mani, R. G.; Smet, J. H.; von Klitzing, K.; Narayanamurti, V.; Johnson, W. B.; Umansky, V. Demonstration of a 1/4-cycle phase shift in the radiation-induced oscillatory magnetoresistance in GaAs/AlGaAs devices. *Phys. Rev. Lett.* **2004**, *92*, 146801.
(47) Abstreiter, G.; Kotthaus, J. P.; Koch, J. F.; Dorda, G. Cyclotron resonance of electrons in surface space-charge layers on silicon. *Phys. Rev. B* **1976**, *14*, 2480.
(48) Fedorych, O. M.; Potemski, M.; Studenikin, S. A.; Gupta, J. A.; Wasilewski, Z. R.; Dmitriev, I. A. Quantum oscillations in the microwave magnetoabsorption of a two-dimensional electron gas. *Phys. Rev. B: Condens. Matter Mater. Phys.* **2010**, *81*, 201302.
(49) Ando, T. Theory of cyclotron resonance lineshape in a two-dimensional electron system. *J. Phys. Soc. Jpn.* **1975**, *38*, 989.
(50) Dmitriev, I. A.; Mirlin, A. D.; Polyakov, D. G. Cyclotron-resonance harmonics in the ac response of a 2D electron gas with smooth disorder. *Phys. Rev. Lett.* **2003**, *91*, 226802.
(51) Briskot, U.; Dmitriev, I. A.; Mirlin, A. D. Quantum magneto-oscillations in the ac conductivity of disordered graphene. *Phys. Rev. B: Condens. Matter Mater. Phys.* **2013**, *87*, 195432.
(52) Dmitriev, I. A.; Khodas, M.; Mirlin, A. D.; Polyakov, D. G.; Vavilov, M. G. Mechanisms of the microwave photoconductivity in two-dimensional electron systems with mixed disorder. *Phys. Rev. B: Condens. Matter Mater. Phys.* **2009**, *80*, 165327.
(53) Dmitriev, I. A.; Dorozhkin, S. I.; Mirlin, A. D. Theory of microwave-induced photocurrent and photovoltage magneto-oscillations in a spatially nonuniform two-dimensional electron gas. *Phys. Rev. B: Condens. Matter Mater. Phys.* **2009**, *80*, 125418.
(54) Ryzhii, V. I. Photoconductivity characteristics in thin films subjected to crossed electric and magnetic fields. *Sov. Phys. Solid State* **1970**, *11*, 2078.


https://dx.doi.org/10.1021/acs.nanolett.0c01918
*Nano Lett.* 2020, 20, 5943−5950

(55) Ryzhii, V. I.; Suris, R. A.; Shchamkhalova, B. S. Photoconductivity of a two-dimensional electron gas in a strong magnetic field. *Sov. Phys. Semicond.* **1986**, *20*, 1299.
(56) Durst, A. C.; Sachdev, S.; Read, N.; Girvin, S. M. Radiation-induced magnetoresistance oscillations in a 2D electron gas. *Phys. Rev. Lett.* **2003**, *91*, No. 086803.
(57) Vavilov, M. G.; Aleiner, I. L. Magnetotransport in a two-dimensional electron gas at large filling factors. *Phys. Rev. B: Condens. Matter Mater. Phys.* **2004**, *69*, No. 035303.
(58) Khodas, M.; Vavilov, M. G. Effect of microwave radiation on the nonlinear resistivity of a two-dimensional electron gas at large filling factors. *Phys. Rev. B: Condens. Matter Mater. Phys.* **2008**, *78*, 245319.
(59) Dmitriev, I. A.; Vavilov, M. G.; Aleiner, I. L.; Mirlin, A. D.; Polyakov, D. G. Theory of microwave-induced oscillations in the magnetoconductivity of a two-dimensional electron gas. *Phys. Rev. B: Condens. Matter Mater. Phys.* **2005**, *71*, 115316.
(60) Dmitriev, I. A.; Mirlin, A. D.; Polyakov, D. G. Oscillatory ac conductivity and photoconductivity of a two-dimensional electron gas: Quasiclassical transport beyond the Boltzmann equation. *Phys. Rev. B: Condens. Matter Mater. Phys.* **2004**, *70*, 165305.
(61) Chepelianskii, A. D.; Shepelyansky, D. L. Microwave stabilization of edge transport and zero-resistance states. *Phys. Rev. B: Condens. Matter Mater. Phys.* **2009**, *80*, 241308.
(62) Mikhailov, S. A. Theory of microwave-induced zero-resistance states in two-dimensional electron systems. *Phys. Rev. B: Condens. Matter Mater. Phys.* **2011**, *83*, 155303.
(63) Beltukov, Y. M.; Dyakonov, M. I. Microwave-induced resistance oscillations as a classical memory effect. *Phys. Rev. Lett.* **2016**, *116*, 176801.
(64) Dorozhkin, S. I.; Dmitriev, I. A.; Mirlin, A. D. Negative conductivity and anomalous screening in two-dimensional electron systems subjected to microwave radiation. *Phys. Rev. B: Condens. Matter Mater. Phys.* **2011**, *84*, 125448.
(65) Dorozhkin, S. I.; Kapustin, A. A.; Umansky, V.; von Klitzing, K.; Smet, J. H. Microwave-induced oscillations in magnetocapacitance:-direct evidence for nonequilibrium occupation of electronic states. *Phys. Rev. Lett.* **2016**, *117*, 176801.
(66) Fu, X.; Ebner, Q. A.; Shi, Q.; Zudov, M. A.; Qian, Q.; Watson, J. D.; Manfra, M. J. Microwave-induced resistance oscillations in a back-gated GaAs quantum well. *Phys. Rev. B: Condens. Matter Mater. Phys.* **2017**, *95*, 235415.
(67) Tabrea, D.; Dmitriev, I. A.; Dorozhkin, S. I.; Gorshunov, B. P.; Boris, A. V.; Kozuka, Y.; Tsukazaki, A.; Kawasaki, M.; von Klitzing, K.; Falson, J. Microwave response of interacting oxide two-dimensional electron systems. 2020, 2006.13627. arXiv/cond-mat.meshall. https://arxiv.org/abs/2006.13627/ (accessed June 24, 2020).
(68) Mani, R. G.; Kriisa, A.; Munasinghe, R. Radiation-induced magnetoresistance oscillations in monolayer and bilayer graphene. *Sci. Rep.* **2019**, *9*, 7278.
(69) Novoselov, K. S.; Geim, A. K.; Morozov, S. V.; Jiang, D.; Katsnelson, M. I.; Grigorieva, I. V.; Dubonos, S. V.; Firsov, A. A. Two-dimensional gas of massless Dirac fermions in graphene. *Nature* **2005**, *438*, 197−200.
(70) Zhang, Y.; Tan, Y.-W.; Stormer, H. L.; Kim, P. Experimental observation of the quantum Hall effect and Berry's phase in graphene. *Nature* **2005**, *438*, 201−204.
(71) Kumaravadivel, P.; Greenaway, M. T.; Perello, D.; Berdyugin, A.; Birkbeck, J.; Wengraf, J.; Liu, S.; Edgar, J. H.; Geim, A. K.; Eaves, L.; Kumar, R. K. Strong magnetophonon oscillations in extra-large graphene. *Nat. Commun.* **2019**, *10*, 3334.
(72) Shi, Q.; Zudov, M. A.; Dmitriev, I. A.; Baldwin, K. W.; Pfeiffer, L. N.; West, K. W. Fine structure of high-power microwave-induced resistance oscillations. *Phys. Rev. B: Condens. Matter Mater. Phys.* **2017**, *95*, No. 041403.
(73) Zeng, Y.; Li, J. I. A.; Dietrich, S. A.; Ghosh, O. M.; Watanabe, K.; Taniguchi, T.; Hone, J.; Dean, C. R. High-quality magnetotransport in graphene using the edge-free Corbino geometry. *Phys. Rev. Lett.* **2019**, *122*, 137701.
(74) Herrmann, T.; Dmitriev, I. A.; Kozlov, D. A.; Schneider, M.; Jentzsch, B.; Kvon, Z. D.; Olbrich, P.; Bel'kov, V. V.; Bayer, A.; Schuh, D.; Bougeard, D.; Kuczmik, T.; Oltscher, M.; Weiss, D.; Ganichev, S. D. Analog of microwave-induced resistance oscillations induced in GaAs heterostructures by terahertz radiation. *Phys. Rev. B: Condens. Matter Mater. Phys.* **2016**, *94*, No. 081301.
(75) Herrmann, T.; Kvon, Z. D.; Dmitriev, I. A.; Kozlov, D. A.; Jentzsch, B.; Schneider, M.; Schell, L.; Bel'kov, V. V.; Bayer, A.; Schuh, D.; Bougeard, D.; Kuczmik, T.; Oltscher, M.; Weiss, D.; Ganichev, S. D. Magnetoresistance oscillations induced by high-intensity terahertz radiation. *Phys. Rev. B: Condens. Matter Mater. Phys.* **2017**, *96*, 115449.
(76) Hatke, A. T.; Zudov, M. A.; Pfeiffer, L. N.; West, K. W. Temperature dependence of microwave photoresistance in 2D electron systems. *Phys. Rev. Lett.* **2009**, *102*, No. 066804.
(77) Ryzhii, V.; Chaplik, A.; Suris, R. Absolute negative conductivity and zero-resistance states in two-dimensional electron systems: A plausible scenario. *JETP Lett.* **2004**, *80*, 363.
(78) Mamani, N. C.; Gusev, G. M.; Lamas, T. E.; Bakarov, A. K.; Raichev, O. E. Resonance oscillations of magnetoresistance in double quantum wells. *Phys. Rev. B: Condens. Matter Mater. Phys.* **2008**, *77*, 205327.
(79) Chaplik, A. V. Energy spectrum and electron scattering processes in inversion layers. *Sov. Phys. JETP* **1971**, *33*, 997.
(80) Giuliani, G. F.; Quinn, J. J. Lifetime of a quasiparticle in a two-dimensional electron gas. *Phys. Rev. B: Condens. Matter Mater. Phys.* **1982**, *26*, 4421.
(81) Krishna Kumar, R.; Bandurin, D. A.; Pellegrino, F. M. D.; Cao, Y.; Principi, A.; Guo, H.; Auton, G. H.; Ben Shalom, M.; Ponomarenko, L. A.; Falkovich, G.; Watanabe, K.; Taniguchi, T.; Grigorieva, I. V.; Levitov, L. S.; Polini, M.; Geim, A. K. Superballistic flow of viscous electron fluid through graphene constrictions. *Nat. Phys.* **2017**, *13*, 1182.
(82) Polini, M.; Vignale, G.The quasiparticle lifetime in a doped graphene sheet. In *No-nonsense physicist: An overview of Gabriele Giuliani's work and life*; edizioni della normale ed.; quaderni selections; Polini, M., Vignale, G., Pellegrini, V., Jain, J. K., Eds.; Scuola Normale Superiore: Pisa, Italy, 2016; Vol. 2, p 107.
(83) Principi, A.; Vignale, G.; Carrega, M.; Polini, M. Bulk and shear viscosities of the two-dimensional electron liquid in a doped graphene sheet. *Phys. Rev. B: Condens. Matter Mater. Phys.* **2016**, *93*, 125410.
(84) Greenaway, M. T.; Krishna Kumar, R.; Kumaravadivel, P.; Geim, A. K.; Eaves, L. Magnetophonon spectroscopy of Dirac fermion scattering by transverse and longitudinal acoustic phonons in graphene. *Phys. Rev. B: Condens. Matter Mater. Phys.* **2019**, *100*, 155120.
(85) Hatke, A. T.; Zudov, M. A.; Pfeiffer, L. N.; West, K. W. Phonon-induced resistance oscillations in 2D systems with a very high electron mobility. *Phys. Rev. Lett.* **2009**, *102*, No. 086808.
(86) Dorozhkin, S. I.; Pfeiffer, L.; West, K.; von Klitzing, K.; Smet, J. H. Random telegraph photosignals in a microwave-exposed two-dimensional electron system. *Nat. Phys.* **2011**, *7*, 336.
(87) Raichev, O. E.; Zudov, M. A. Effect of Berry phase on nonlinear response of two-dimensional fermions. *Phys. Rev. Research* **2020**, *2*, No. 022011.
(88) Chepelianskii, A. D.; Shepelyansky, D. L. Floquet theory of microwave absorption by an impurity in the two-dimensional electron gas. *Phys. Rev. B: Condens. Matter Mater. Phys.* **2018**, *97*, 125415.


https://dx.doi.org/10.1021/acs.nanolett.0c01918
*Nano Lett.* 2020, 20, 5943−5950